Recent trends of the tropical hydrological cycle inferred from Global Precipitation Climatology Project and International Satellite Cloud Climatology Project data

Y. P. Zhou,[1,2] Kuan-Man Xu,[3] Y. C. Sud,[2] and A. K. Betts[4]

Received 15 October 2010; revised 4 January 2011; accepted 7 February 2011; published 7 May 2011.

[1] Scores of modeling studies have shown that increasing greenhouse gases in the atmosphere impact the global hydrologic cycle; however, disagreements on regional scales are large, and thus the simulated trends of such impacts, even for regions as large as the tropics, remain uncertain. The present investigation attempts to examine such trends in the observations using satellite data products comprising Global Precipitation Climatology Project precipitation and International Satellite Cloud Climatology Project cloud and radiation. Specifically, evolving trends of the tropical hydrological cycle over the last 20–30 years were identified and analyzed. The results show (1) intensification of tropical precipitation in the rising regions of the Walker and Hadley circulations and weakening over the sinking regions of the associated overturning circulation; (2) poleward shift of the subtropical dry zones (up to 2° decade^{-1} in June-July-August (JJA) in the Northern Hemisphere and 0.3–0.7° decade^{-1} in June-July-August and September-October-November in the Southern Hemisphere) consistent with an overall broadening of the Hadley circulation; and (3) significant poleward migration (0.9–1.7° decade^{-1}) of cloud boundaries of Hadley cell and plausible narrowing of the high cloudiness in the Intertropical Convergence Zone region in some seasons. These results support findings of some of the previous studies that showed strengthening of the tropical hydrological cycle and expansion of the Hadley cell that are potentially related to the recent global warming trends.

Citation: Zhou, Y. P., K.-M. Xu, Y. C. Sud, and A. K. Betts (2011), Recent trends of the tropical hydrological cycle inferred from Global Precipitation Climatology Project and International Satellite Cloud Climatology Project data, *J. Geophys. Res.*, *116*, D09101, doi:10.1029/2010JD015197.

1. Introduction

[2] Among the greenhouse gas–induced climate change projections, tropical hydrological cycle changes can be expected to cause shortage or excess of precipitation in many regions and that in turn would impact all life: human, animal, and plant. Recent studies provide contradictory guidance about the evolving trends in the tropical circulations. At least two reanalysis data sets, namely the National Centers for Environmental Prediction/National Center for Atmospheric Research (NCEP/NCAR) and the European Center for Medium-Range Weather Forecast (ECMWF) Reanalysis (ERA40), show strengthening trends of the Hadley circulation [*Quan et al.*, 2004; *Tanaka et al.*, 2004; *Mitas and Clement*, 2005, 2006] over the last few decades. However, general circulation models (GCMs) simulating the influence of increased greenhouse gases produce weakening of the tropical overturning circulation that affects the Walker circulation more strongly than the Hadley circulation [*Mitas and Clement*, 2006; *Held and Soden*, 2006; *Vecchi et al.*, 2006; *Vecchi and Soden*, 2007]. These simulation results are consistent with heuristic arguments suggesting that whereas the atmospheric moisture at fixed relative humidity increases at ~7% °C^{-1} (following the Clausius-Clapeyron relation) [*Held and Soden*, 2006], the global mean precipitation, governed by radiative-convective balance, increases at less than half this rate. Therefore, a weaker overturning circulation must occur in response to the warming environment to match the radiative constraints on evaporation and precipitation [*Betts and Ridgway*, 1989; *Betts*, 1998; *Knutson and Manabe*, 1995; *Allen and Ingram*, 2002; *Held and Soden*, 2006; *Sud et al.*, 2008]. Locally, precipitation and moist convection could be enhanced in convective (wet) regions following the "rich-get-richer mechanism" because gross moist stability is reduced when the increase of moisture is concentrated mainly in the lower troposphere [*Chou and Neelin*, 2004; *Chou et al.*, 2009].

[1]Goddard Earth Sciences and Technology Center, University of Maryland, Baltimore County, Catonsville, Maryland, USA.
[2]Laboratory for Atmospheres, NASA Goddard Space Flight Center, Greenbelt, Maryland, USA.
[3]Climate Science Branch, Science Directorate, NASA Langley Research Center, Hampton, Virginia, USA.
[4]Atmospheric Research, Pittsford, Vermont, USA.

0148-0227/11/2010JD015197

[3] One plausible explanation of the contradiction between the reanalyses and the GCM simulations is that the radiosonde profiles that went into the reanalyses had a cooling trend in the upper atmosphere [*Santer et al.*, 2005] and that cooling trend remaining in the reanalyses might have reduced the atmospheric stability and enhanced the vertical motion [*Mitas and Clement*, 2006]. *Uppala et al.* [2005] suggest that it was the satellite humidity analysis that was responsible for the upward drift of precipitation in ERA-40. On the other hand, the simulated thermal structure and corresponding circulations depend on GCMs' physical parameterizations, which may be problematic [*Randall et al.*, 2003] and cause systematic biases in thermal structures in the present-day GCMs. Such systematic differences between GCM simulations and reanalysis data underline the importance of using observational data for ascertaining the long-term trends of the tropical circulation and the associated hydrological cycle [*Wielicki et al.*, 2002; *Chen et al.*, 2002; *Zhang and Song*, 2006; *Wentz et al.*, 2007]. This provides the primary motivation for the current study.

[4] More recently, observational data analyses have shown a broadening of the Hadley cell, which have been inferred from the metrics of trends in tropopause height [*Reichler and Held*, 2005; *Fu et al.*, 2006; *Seidel and Randel*, 2007], atmospheric ozone [*Hudson et al.*, 2006], water vapor transport [*Sohn and Park*, 2010] and outgoing longwave radiation (OLR) [*Hu and Fu*, 2007], as well as an index of Hadley circulation [*Hu and Fu*, 2007; *Lu et al.*, 2007]. *Seidel et al.* [2008] suggested that the Hadley cell have broadened by 2–4° since 1979.

[5] An important question that is yet to be addressed is the following. How do changes in tropical circulation and variously inferred expansion of the Hadley cell affect the tropical hydrological cycle? Although closely related, one must distinguish between the trends in tropical circulation and tropical hydrological cycle, which is characterized by total precipitation and its spatial and temporal distributions. We must point out that even a weakening tropical overturning circulation does not necessarily imply weakening of the hydrological cycle. Indeed, some studies have shown increases in both total precipitation and extreme precipitation episodes in the tropics, and increasing contrast between the wet and dry regions, indicating strengthening of the overall hydrological cycle [*Wang and Lau*, 2005; *Lau and Wu*, 2007; *Allan and Soden*, 2008].

[6] In this study, we use the Global Precipitation Climatology Project (GPCP) monthly precipitation data [*Adler et al.*, 2003] and the International Satellite Cloud Climatology Project (ISCCP) version FD cloud and radiation data [*Zhang et al.*, 2004] to examine the changes in tropical precipitation, cloud and radiation fields associated with tropical overturning circulations. We also define proxies for the latitudinal extent of the Hadley cell, examine its long-term variability and discuss the associated implications for the tropical hydrological cycle.

[7] The rest of the paper is organized as follows. Section 2 describes the data sets used in the study. Section 3 examines the trends in precipitation distributions associated with Walker and Hadley circulations and expansion of Hadley cell using precipitation as a proxy. Section 4 analyzes cloudiness and top of the atmosphere (TOA) radiation data to examine the Hadley cell expansion and infer the changes in the tropical hydrological cycle. Section 5 provides a summary and discussion of the results.

2. Data

[8] The Global Precipitation Climatology Project (GPCP) monthly precipitation data product (version 2.1) is a community-based analysis of global precipitation under the auspices of the World Climate Research Program (WCRP) [*Adler et al.*, 2003]. The data product spans from 1979 to the present and is archived at 2.5° × 2.5° grid resolution. It merges rainfall estimates from various satellites including microwave-based estimates from Special Sensor Microwave/Imager (SSM/I), infrared (IR) rainfall estimates from geostationary and polar-orbiting satellites, and surface rain gauges. The GPCP data analysis preserves temporal homogeneity by well-designed algorithms mitigating the data inhomogeneity owing to changes in satellites and rainfall algorithms, especially the addition of SSM/I instruments after 1988. The monthly GPCP data has been cross-calibrated before 1988 (pre-SSM/I) with the later period (post-SSM/I) on the basis of an overlapping period to minimize the systematic bias [*Adler et al.*, 2003]. *Smith et al.* [2006] showed that the impact of temporal inhomogeneity of sampling is not a major concern.

[9] The International Satellite Cloud Climatology Project (ISCCP), also a WCRP project, analyzes satellite radiance measurements to infer the global distribution of clouds and their roles in climate [*Rossow and Schiffer*, 1999]. It has produced equal-area gridded (2.5° × 2.5°) 3 hourly and monthly cloud products from July 1983 to the present. ISCCP has also produced a version of global radiative flux data product (ISCCP-FD), which was created by employing the radiative transfer code of NASA GISS GCM and ISCCP cloud products [*Zhang et al.*, 2004]. The model also uses a collection of global data sets describing atmospheric and surface properties such as the daily atmospheric temperature and humidity from National Oceanic and Atmospheric Administration (NOAA) Television Infrared Observation Satellites (TIROS) Operational Vertical Sounder and daily ozone abundances from Total Ozone Mapping Spectrometer as input for the flux calculations. Originally designed to study the clouds in synoptic weather systems, the ISCCP FD data have been used in a number of decadal and longer-term climate change analysis [*Chen et al.*, 2002; *Wang and Lau*, 2005; *Clement et al.*, 2009; *Tselioudis et al.*, 2010] as its data period has lengthened.

[10] It has been suggested that the long-term trend of ISCCP cloud amounts may be affected by spatial and temporal inhomogeneity in satellite viewing zenith angle [*Norris*, 2000; *Campbell*, 2004; *Evan et al.*, 2007; *Clement et al.*, 2009]. This is because ISCCP cloud estimates utilize IR and visible radiance information from a series of geostationary and polar-orbiting satellites with varying time spans. Cloud amount tends to be overestimated at higher viewing zenith angle [*Minnis*, 1989]. The viewing zenith angle from geostationary satellite increases from nadir to the edge of the footprint, therefore, as satellite configuration changes over the time (that is, launch of new satellites, reposition or disabling of existing satellites), viewing zenith angles can change, which may bring artificial changes in cloud amount. To minimize spatial inhomogeneity, ISCCP

uses nearest geostationary satellite measurements when possible, supplemented by AVHRR measurements from polar-orbiting satellite when geostationary satellite measurements are not available, for latitudes poleward of 60° north and south. There is a segment of the Indian Ocean where geostationary satellite coverage did not exist until the late 1990s and data from the AVHRR was employed. The drifting of equatorial crossing time (ETC) of polar orbiting satellites has been found to affect the derived OLR and Highly Reflective Cloud (HRC) fields [*Waliser and Zhou*, 1997; *Lucas et al.*, 2001] mainly owing to the diurnal cycle in the cloud field. Since a polar-orbiting satellite has constantly varying viewing zenith angle at each location, the effect of viewing zenith angle tends to cancel out in the monthly data [*Campbell*, 2004]. Nevertheless, large artificial jumps could occur when AVHRR is replaced by geostationary measurements.

[11] The ISCCP computed radiative fluxes, which are an integral of many atmospheric, cloud and surface properties were not dominated by any single input as shown by *Hinkelman et al.* [2009]. To account for the plausible artifacts in the ISCCP cloudiness due to the above effects, we conducted trend analysis associated with Hadley cell expansion using the full set of data as well as its subsets data with minimal artifacts. In addition to the ISCCP FD data, where we obtained monthly gridded TOA radiation fluxes and cloud amount, we calculated monthly averaged viewing zenith angle from ISCCP D1 data set, which is a 3 hourly equal-area gridded data. The monthly viewing zenith angle is used to mask out large biased areas.

3. Trends of Tropical Hydrological Cycle Inferred From the GPCP Data

[12] To examine the precipitation trends and their geographical distribution, two types of monthly precipitation anomalies were produced with the GPCP data: one by subtracting the monthly climatology and thus the mean annual cycle from the data (called Anom-I), another by further removing El Niño–Southern Oscillation (ENSO) effects using regression to the Nino3.4 index (monthly SST anomaly over the region 5°N–5°S, 120°–170°W) provided by the NCEP Climate Prediction Center (called Anom-II). The monthly anomalous time series are summed to seasonal and annual time series and a linear trend was computed for each grid box. The geographical distributions of such trends in the annual precipitation (background shaded) were computed with Anom-I (Figure 1a) and Anom-II (Figure 1b) data for the tropics over a 29 year (1979–2007) period. The climatology of the same period is superimposed as contours in Figures 1a and 1b. The linear trend (contour) and the confidence level (background shade) from a student *t* test for the Anom-II data are shown in Figure 1c.

[13] Figures 1a–1c show that the majority of the tropical areas exhibit trends of increasing precipitation; the strongest positive trends are seen in the heavy precipitation areas (i.e., Intertropical Convergence Zone (ITCZ), South Pacific Convergence Zone (SPCZ), Indian Pacific warm pool, and the Amazon regions), while the strongest negative trends are noted over the light precipitation area (i.e., at both edges of the ITCZ, south of equatorial Africa; see Figure 1a). The trend distribution of the ENSO-removed data shows a very similar spatial pattern with the one that contains ENSO effect, with slightly stronger trends in the areas with large positive and negative trends (Figure 1b). The trends over the majority of the areas show better than 90% confidence level, especially in the subtropical sinking area in northeast Pacific, tropical Indian Ocean and African continent (Figure 1c). The student's *t* test used in this study uses lag-1 correlation in defining the degree of freedom to remove the autocorrelation in the time series [*Santer et al.*, 2000; *Gu et al.*, 2007]. Figure 1 shows that wet (dry) regions tend to become wetter (drier), in agreement with a number of recent studies [*Allan and Soden*, 2007; *Chou et al.*, 2007; *Lau and Wu*, 2007; *Zhang et al.*, 2007; *Sohn and Park*, 2010]. There arises a need to address another fundamental question: how are these trends related to the changes in the tropical Walker and Hadley circulations?

3.1. Precipitation Distribution Trend Associated With the Walker Circulation

[14] This section examines precipitation changes associated with the Walker circulation. We base our findings on meridionally averaged (30°N–30°S) precipitation fields for each season together with their annual mean trends. Figure 2 shows a time-longitude cross section of annual mean precipitation averaged from 30°N to 30°S and the corresponding trend for each longitude. Heavy precipitation over the Indian and Western Pacific Oceans in the 90–180°E region corresponds to the rising branches of the Walker circulation over both oceans. Relatively heavy precipitation over the Atlantic Ocean in the 40–70°W region corresponds to the rising branch of the Atlantic Walker circulation. Light precipitation is found over the 90–150°W and 0–30°W regions corresponding to the sinking branch of the Pacific and Atlantic Walker circulations, respectively. The lowest precipitation is found over continental Africa and West India Ocean, in particular, the 15°W to 10°E region.

[15] The zonal distribution of the 29 year trend shows that positive trends over the rising regions of the three Walker circulations, namely the Pacific, Indian and Atlantic Walker circulations, and negative trends appear in the regions of light precipitation. Table 1 shows that the linear trends of precipitation (for Anom-I data) over the rising (120–180°E) and sinking (90–150°W) regions of the Pacific Walker circulation are positive and negative, respectively, for all the seasons and annual mean, with March-April-May (MAM) and June-July-August (JJA) having the largest positive trends with above 95% confidence level (c.l.) based on student's *t* test (Table 1). The computed annual mean trend in the rising region is 0.113 mm d^{-1} $decade^{-1}$ and −0.065 mm d^{-1} $decade^{-1}$ in the sinking region. The precipitation trends computed from Anom-II time series (with ENSO effects removed) shows the same positive (negative) trends in the rising (sinking) regions of the Walker circulation, with only slightly smaller magnitudes from the December-January-February (DJF), MAM, and September-October-November (SON) but generally improved statistical significance, especially for MAM, JJA and annual mean in the sinking region (Table 1).

[16] Recent studies using reanalysis data sets show that the zonal mass circulation intensity of the Walker circulations over the Indian and Atlantic Oceans have been strengthening in recent decades while the Pacific Walker

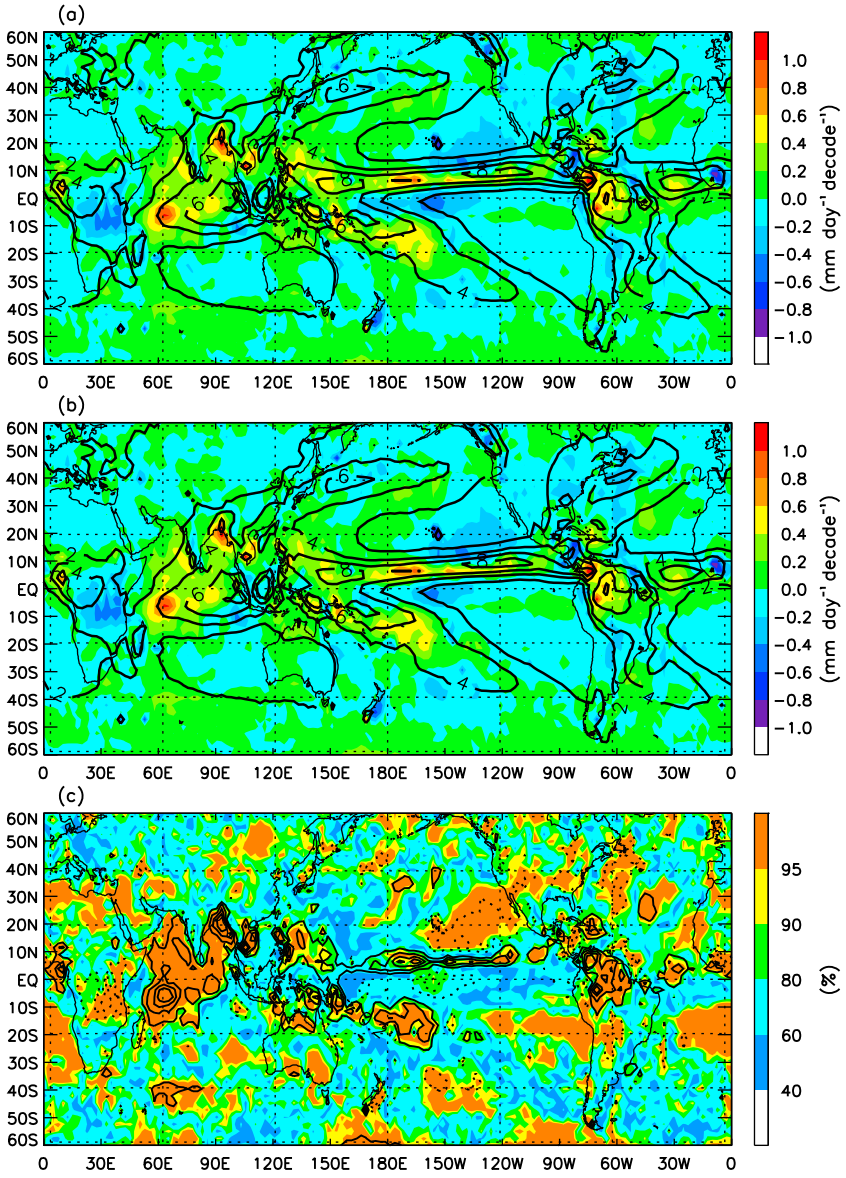

Figure 1. GPCP climatology (contour) overlaid with linear trends (shading) from deseasonalized time series (a) with ENSO signal and (b) ENSO signal removed. (c) Linear trend from Figure 1b (contour) and the confidence level (shading).

circulation has been weakening [*Zhao and Moore*, 2008; *Yu and Zwiers*, 2010]. Note that the latitudinal extent used in defining the Walker circulations was much narrower (5°S to 5°N; 0 to 20°N) than that used in this study (30°S to 30°N). The weakening of the Pacific Walker circulation intensity was at maximum around the dateline but the rising branch of the Walker circulation west of 140°E were strengthened [*Zhao and Moore*, 2008]. We examined selected regions over the Indian and Atlantic Ocean and found that precipitation associated with the rising branches of the Walker circulations has increased uniformly while precipitation associated with the sinking branch of the Walker circulation has either decreased (over the Atlantic Ocean) or has an insignificant change (over the Indian Ocean) (figures not shown). This results in an increasing trend of total precipitation in the tropics [*Gu et al.*, 2007]. Overall, the precipitation distribution associated with the Walker circulation tends to have increased contrasts between the wet and dry regions. This result may be related to increasing low-level moisture transport from drier to moister regions [*Sohn and Park*, 2010], which is coupled with vertical moisture advection that is induced by relatively stronger low-level moisture increase and weaker high-level moisture increase; that is, a thermodynamic component such as in the work of *Held and Soden* [2006] and *Chou et al.* [2009].

3.2. Precipitation Distribution Trend Associated With the Hadley Circulation

[17] The changes in precipitation distribution associated with the Hadley circulation are investigated using zonally averaged precipitation. The time-latitude cross section of the annual mean precipitation shows a large band of high pre-

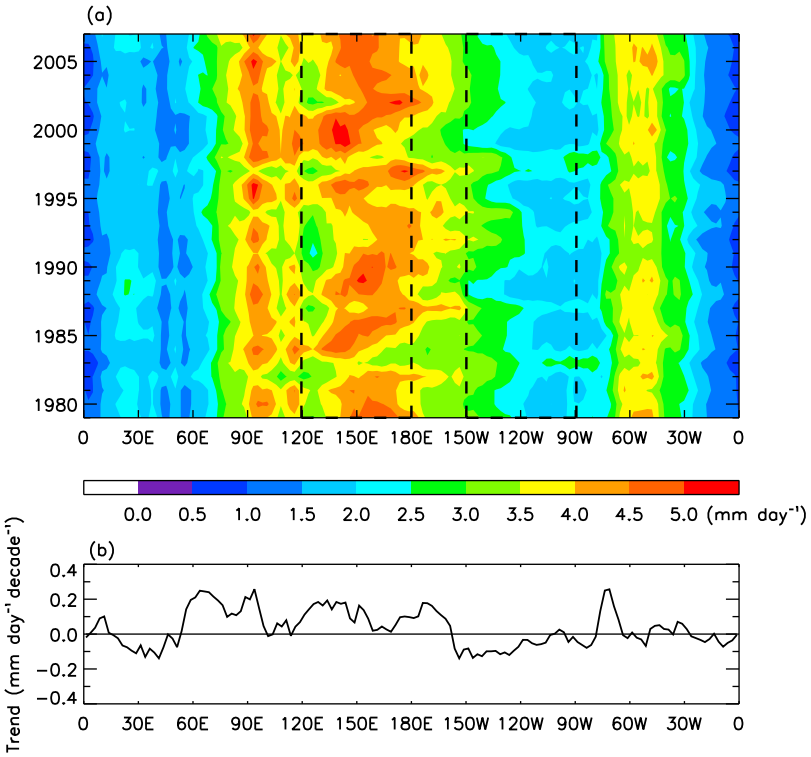

Figure 2. (a) Time-longitude distribution of meridionally averaged (30°S–30°N) GPCP annual mean precipitation. (b) Corresponding linear trend with longitude. The rising and sinking areas of the Pacific Walker circulation are marked.

cipitation in the ascending region of the ITCZ and a band of small precipitation in the subtropical subsidence region(s) (Figure 3a). The latitudinal distribution of precipitation trends shows a positive trend in the 15°S–25°N region that peaks around 5°N, where ITCZ rains most, and negative trends in the subtropical sinking region(s) (Figure 3b). The negative trend in the Northern Hemisphere extends to about 55°N which is likely due to decreases of precipitation associated with midlatitude storm tracks [*Yin*, 2005] and a northward shift of the Hadley circulation [*Lu et al.*, 2007]. The latter will be further discussed in section 3.3.

[18] Using a similar methodology for the Walker circulation, the precipitation trends for the tropical rising region (17.5°S–17.5°N) and the subtropical sinking regions in the Northern (17.5–40°N) and Southern (35–17.5°S) Hemispheres are computed for each season and the annual mean precipitation using Anom-I and Anom-II data (Table 2), respectively. It is found that the tropical rising region displays a significant positive trend of rainfall rates in all the seasons; its magnitude is between 0.057 and 0.085 mm d^{-1} $decade^{-1}$. For the subtropical sinking regions, it is interesting to note that the winter and spring seasons in each hemisphere had significant negative trends while the summer and fall seasons had slight positive trends, but lacked statistical significance. The annual mean precipitation has a significant positive trend of 0.067 mm d^{-1} $decade^{-1}$ in the rising region and negative trends of −0.15 and −0.018 mm d^{-1} $decade^{-1}$ in the Northern and Southern Hemispheres, respectively, at a marginal 90% c.l. (Table 2). This increasing rainfall in the rainy ITCZ region and decreasing rainfall in the dry subtropical sinking region(s) indicates strengthening of the hydrological cycle in the tropics. The long-term trends of

Table 1. Precipitation Trends Associated With the Walker Circulation in the Rising and Sinking Regions With and Without ENSO Signal[a]

Trend (mm $d^{-1}$$decade^{-1}$)	December-January-February	March-April-May	June-July-August	September-October-November	Annual
		With ENSO Signal			
Rising region (30°S–30°N, 120–180°E)	0.064	*0.177*	*0.113*	*0.088*	*0.113*
Sinking region (30°S–30°N, 150–90°W)	−0.055	−0.089	−0.045	−0.059	−0.065
		ENSO Signal Removed			
Rising region (30°S–30°N, 120–180°E)	0.046	*0.163*	*0.120*	**0.077**	*0.099*
Sinking region (30°S–30°N, 150–90°W)	−0.034	**−0.074**	**−0.054**	−0.047	**−0.052**

[a]Boldface indicates confidence level greater than 90%; italics confidence level greater than 95%.

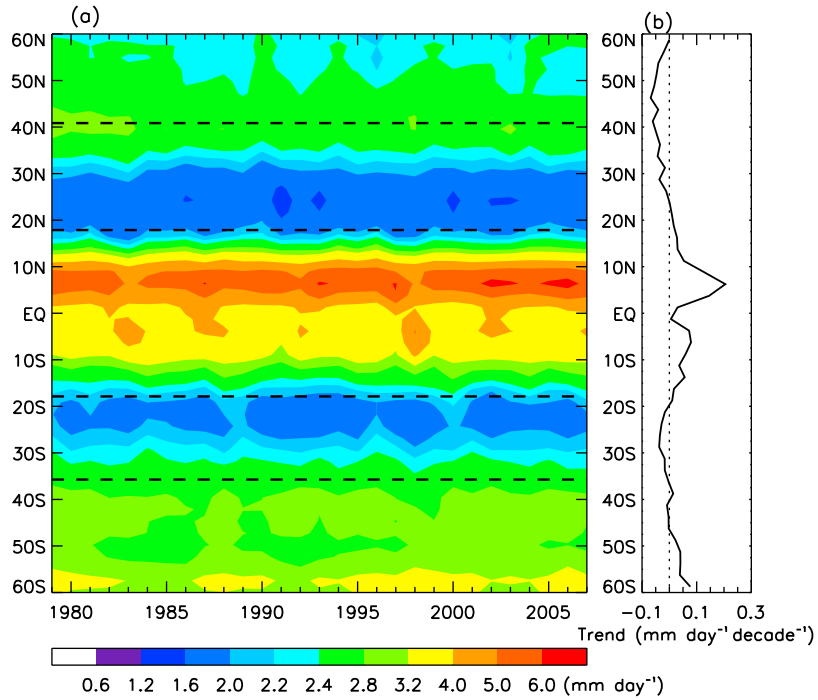

Figure 3. (a) Time-latitude distribution of zonally averaged GPCP annual mean precipitation. (b) Corresponding linear trend with the latitude.

precipitation in the tropics from the ENSO removed data are quite similar, probably owing to cancellation of opposite effects of El Niño and La Niño on precipitation [*Chou and Lo*, 2007]. The asymmetry effect of ENSO on precipitation in the Northern and Southern Hemispheres [*Chou and Lo*, 2007] can be seen in slightly smaller precipitation trends in the Southern Hemisphere in the ENSO removed trends (Table 2).

3.3. Expansion of Hadley Circulation Evidenced From GPCP Data

[19] Figure 3 shows the meridional distribution of annual mean zonal precipitation as well as the approximate locations of the ITCZ, the subtropical dry band, and the extremities of the Hadley cell. To discern key features of the Hadley circulation, we used a nominal threshold of 2.4 mm d^{-1} to identify the boundaries of the subtropical dry band of the Hadley cell for each season (i.e., Figure 4 for the Northern Hemisphere only). The outer boundary marks the dry subtropical subsidence region from the rainy region of the midlatitude storm track while the inner boundary (closer to the equator) separates the subsidence region from the ITCZ; thus these boundaries can be used as proxies for the Hadley cell and the ITCZ regions. The latitude of minimum precipitation represents the driest (and usually central) position of the dry band.

[20] The Hadley cell boundaries, as defined above, are similar to those inferred from OLR with a 250 W m^{-2} threshold [*Hu and Fu*, 2007] (red dashed line in Figure 4). Figure 4 also shows that the location and width of the dry band for each season; it is located approximately between 10°N and 30°N in DJF and MAM in the Northern Hemisphere, shifts to the higher latitudes in JJA and gets narrower in SON (20–30°N). Despite large interannual variabilities of these boundaries, particularly in JJA, some trends are also

Table 2. Precipitation Trends Associated With the Hadley Circulation in the Rising and Sinking regions in the Northern and Southern Hemispheres with and Without ENSO Signal[a]

Trend (mm d^{-1}decade^{-1})	December-January-February	March-April-May	June-July-August	September-October-November	Annual
		With ENSO Signal			
Sinking region, Northern Hemisphere (17.5–40°N)	*−0.062*	*−0.039*	0.020	0.016	−0.015
Rising region (17.5°S–17.5°N)	*0.085*	*0.058*	*0.057*	*0.068*	*0.067*
Sinking region, Southern Hemisphere (17.5–35°S)	0.018	0.010	*−0.034*	*−0.072*	**−0.018**
		ENSO Signal Removed			
Sinking region, Northern Hemisphere (17.5–40°N)	*−0.062*	*−0.038*	0.020	0.016	−0.014
Rising region (17.5°S–17.5°N)	*0.085*	*0.058*	*0.058*	*0.068*	*0.067*
Sinking region, Southern Hemisphere (17.5–35°S)	0.014	0.008	*−0.033*	*−0.074*	*−0.020*

[a]Boldface indicates confidence level greater than 90%; italics confidence level greater than 95%.

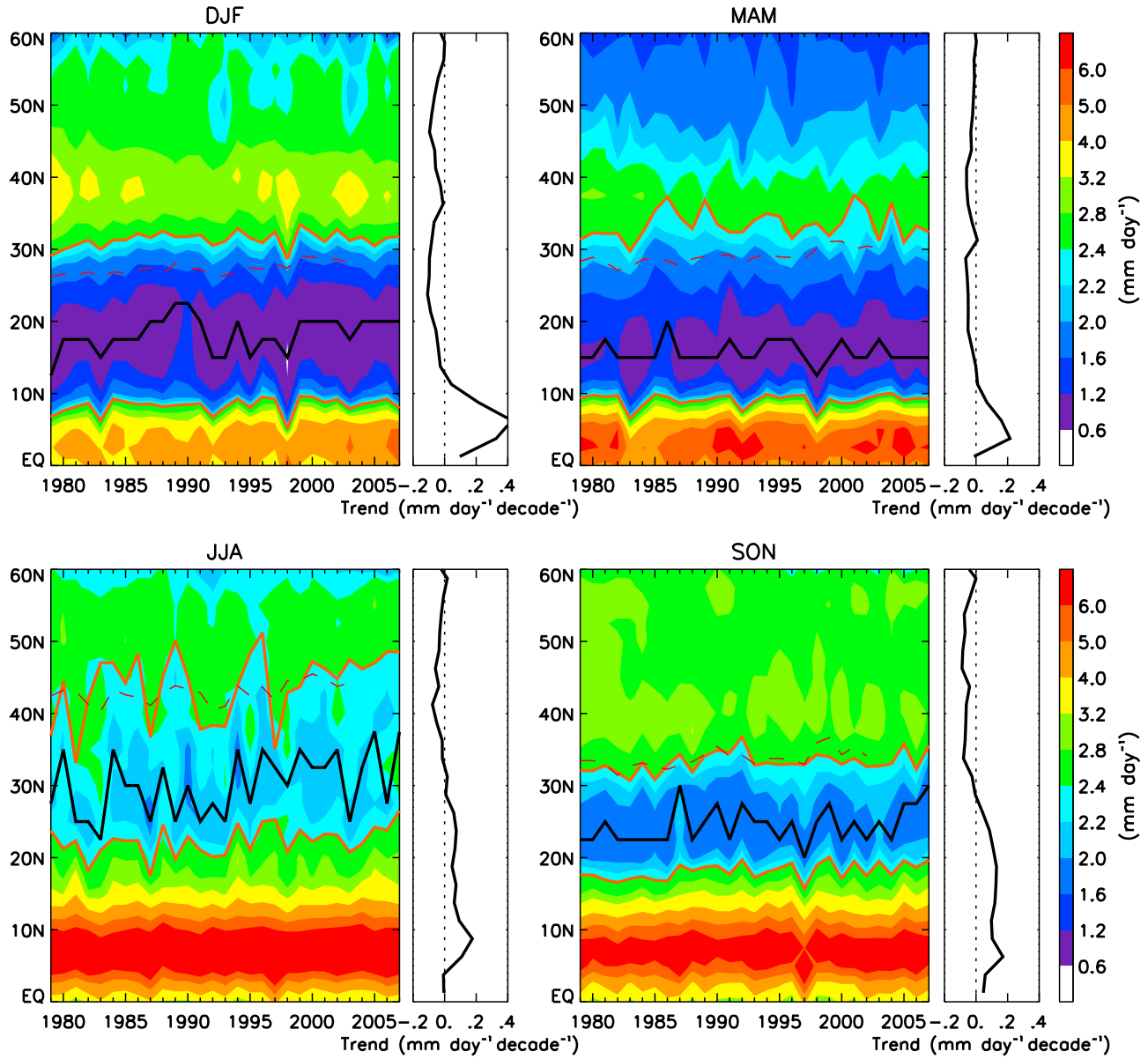

Figure 4. Time-latitude cross sections of zonal mean seasonal precipitation and the corresponding linear trend with latitude. Solid orange lines mark the 2.4 mm d^{-1} precipitation threshold which is used as the boundaries of subtropical dry band. The boundary at the high and low latitude of the dry band is used as a proxy of the boundary of Hadley cell and ITCZ, respectively. Solid black lines indicate latitude with minimum precipitation. Dashed red lines mark the Hadley cell boundary determined by the 250 Wm^{-2} threshold using HIRS OLR data.

evident in the respective time series. Figure 5 summarizes the total trends (or total migration computed from the 29 year linear fit) of the Hadley cell and ITCZ boundaries as well as the position of minimum precipitation for each season and their annual means in both hemispheres. In the Northern Hemisphere, the trends of Hadley cell and ITCZ boundaries reveal a significant northward migration in all the seasons except MAM (Figure 5a; also see Figure 4); these changes are accompanied by a significant northward shift of the minimum precipitation as well. The largest northward expansion of about 6° occurs in JJA, which is likely related to a northward shift of the jet stream in the boreal summer [*Yin*, 2005; *Hu and Fu*, 2007]. For DJF and SON, the northern edges of the ITCZ and Hadley cell boundaries reveal a northward shift of ~1–2° and the minimum precipitation shifts of ~3° northward (the c.l. of DJF is slightly lower than 95%). This has significant implications for ecosystems of the midlatitudes particularly because the majority of the trends are due to the contribution of the land regions (figures not shown).

[21] In the Southern Hemisphere, the Hadley cell and ITCZ also migrates poleward, but the magnitude of the change is much smaller (Figure 5b). Noteworthy trends include a poleward shift of the Hadley cell of 1.3° in JJA (99.9% c.l.) and 2.2° in SON (90.5% c.l.). This is accom-

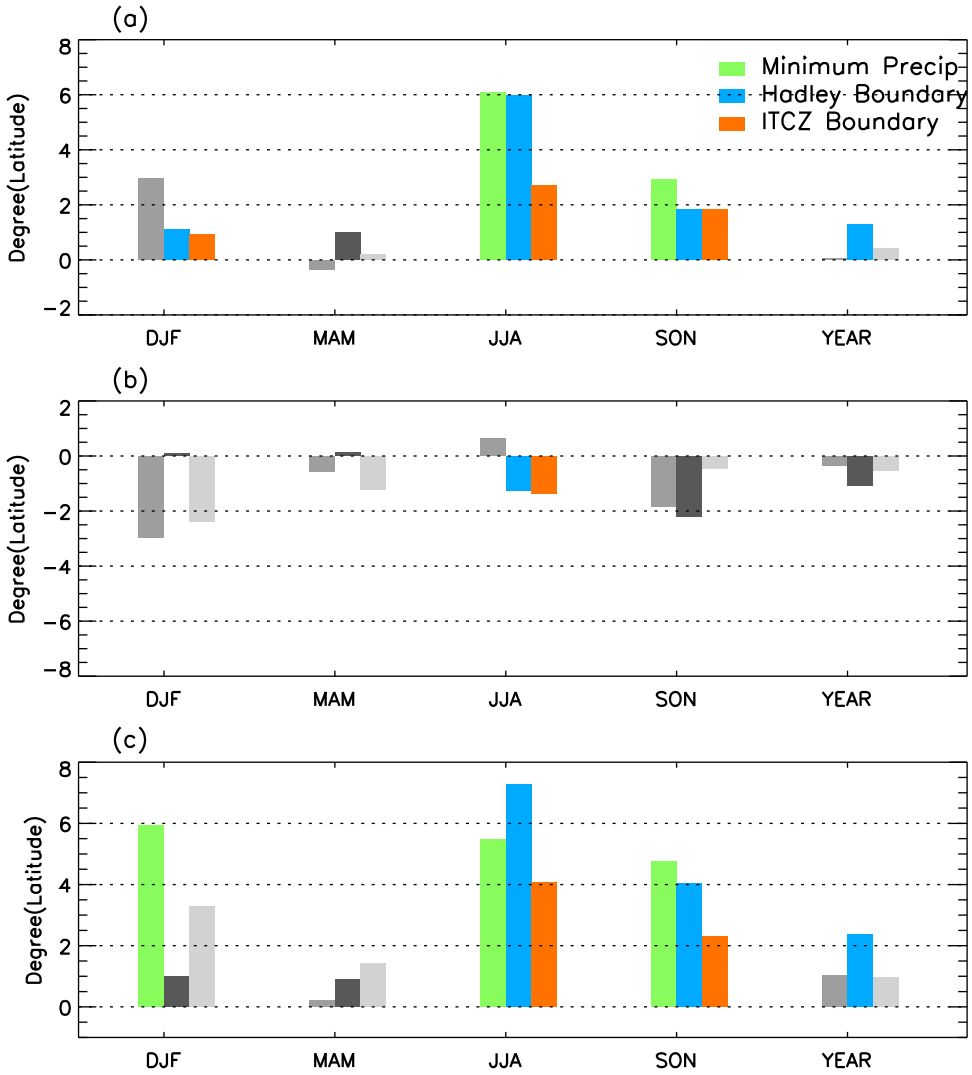

Figure 5. Linear trends of the latitude of minimum precipitation, ITCZ, and Hadley cell boundaries inferred from GPCP for each season and the year marked on the horizontal axis for (a) the Northern Hemisphere and (b) the Southern Hemisphere. (c) Total expansion of the tropics. Leftmost, middle, and rightmost bars in each group are for minimum precipitation, Hadley cell, and ITCZ boundary, respectively. For quantities significant at the 90% level, bars are shaded green, blue, and orange, respectively.

panied by a poleward shift of the ITCZ boundary in all four seasons; however, only JJA has >95% c.l.. The entire tropical expansion, defined by the latitudinal width between the northern and the southern edges of the ITCZ, the locations of minimum precipitation and the Hadley cell are shown in Figure 5c. It shows that the tropical regions have expanded in each of the four seasons, but significant trends are found in JJA and SON only, with a magnitude ranging from 2 to 7 degrees based on the three indices defined above. In the annual mean, only the Hadley boundary has a significant expansion trend of 2.2°.

3.4. Regional Hadley Circulation

[22] The strength and latitudinal extent of the Hadley circulation not only varies with the season but also from region to region [*Waliser and Gautier*, 1993; *Waliser and Somerville*, 1994; *Hou*, 1998; *Webster et al.*, 1998; *Waliser et al.*, 1999; *Zhao and Moore*, 2008]. Here we examine the trends in precipitation distribution for four selected regions in the Northern Hemisphere, namely: HC1 (80–150°E), HC2 (150–240°E), HC3 (240–320°E), and HC4 (0–50°E); these represent major climatologically distinct regions; that is, Asian monsoon and continental region, Pacific Ocean region, North American monsoon and continental region, and continental African region. Figure 6 shows the time-latitude cross sections of zonally averaged precipitation in JJA for each of the four regions and the boundaries of the dry band defined by the same precipitation threshold. As expected, total precipitation amount and dry band locations vary significantly from one region to another. For example, the continental Asian monsoon region has the highest precipitation amount in JJA and the dry band is narrowly located between 40°N to 45°N; the continental African region has the lowest amount of total precipitation in JJA and the dry band is widespread from 15°N to 45°N.

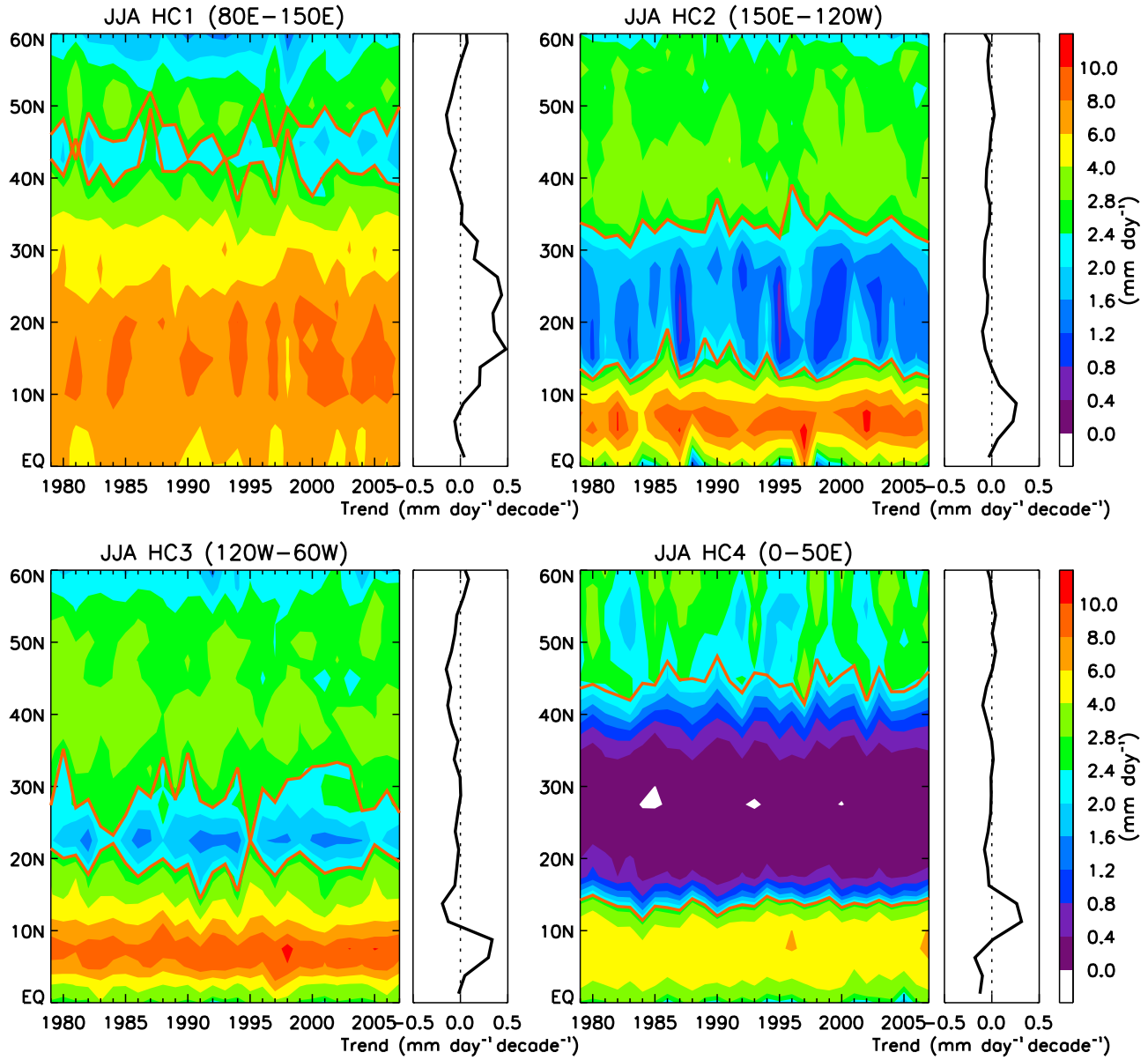

Figure 6. Time-latitude cross sections of zonal mean JJA precipitation and the corresponding linear trend with latitude. Solid orange lines mark the 2.4 mm d^{-1} precipitation threshold which is used as the boundaries of subtropical dry band. The boundary at the high and low latitude of the dry band is used as a proxy of the boundary of Hadley cell and ITCZ, respectively.

[23] Using the same precipitation threshold for identifying the ITCZ and Hadley cell boundaries, the trends for each of these boundaries are shown in Figure 7. The trends for all four regional boundaries of the Hadley cells are positive while all the ITCZ boundaries except for HC4 are negative (i.e., shrinking toward the equator); this shows that the dry bands have expanded in all the four regions in JJA. Among them, only the trends for the HC1 region are significant at above 90% c.l., possibly owing to weakening of the Asian summer monsoon in recent decades that characterized with floods in southern China and dryness in northern China [*Li et al.*, 2010; *Zhao et al.*, 2010]. Also, a large positive trend between 15°N and 25°N might have contributed most to the northward shift of zonal averaged ITCZ boundary in JJA in Figure 4. The low confidence levels for the other regions are partly due to the difficulty in defining the regional boundaries and the large interannual variability in the precipitation for small regions.

4. Hydrological Cycle Changes From ISCCP Data

[24] Clouds are an important component of the Earth's energy and water cycle. Changes in the tropical hydrological cycle would inevitably be seen in the cloud and radiation fields. *Chen et al.* [2002] explored the radiation measurements from the Earth Radiation Budget Experiment (ERBE) and the Clouds and Earth's Radiant Energy System (CERES) and cloud measurements from ISCCP to connect decadal changes in the tropical dynamical system. Despite

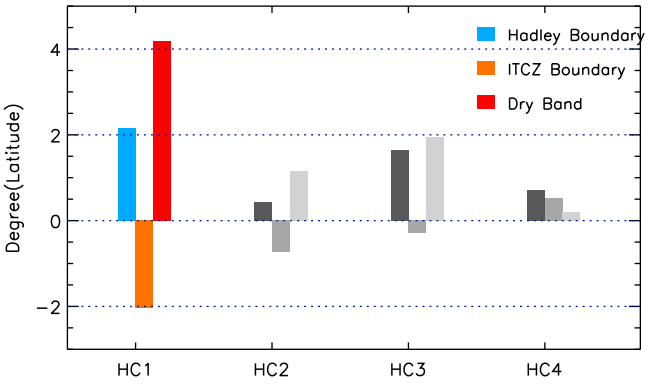

Figure 7. Linear trends for the boundary of Hadley cell, ITCZ, and width of dry band in JJA for the Northern Hemisphere. Leftmost, middle, and rightmost bars in each group are for Hadley cell, ITCZ boundary, and width of dry band, respectively. For quantities significant at the 90% level, bars are shaded blue, orange, and red, respectively.

some concerns about the spatial-temporal inhomogeneity associated with the ISCCP clouds, the ISCCP data are among the best quality-controlled global long-term data products available to date [*Rossow and Schiffer*, 1999; *Zhang et al.*, 2004]. We examine trends in the ISCCP cloudiness and radiation data to infer changes in the tropical hydrological cycle, in connection with the precipitation trends discussed earlier.

4.1. Expansion of Hadley Circulation Evidenced From ISCCP Cloudiness

[25] One may argue that the Hadley cell boundaries inferred from a fixed OLR threshold may also reflect the expansion of the Hadley circulation [*Hu and Fu*, 2007] because of the strong dependency of OLR on cloud and moisture distributions. Here we use instead the ISCCP cloud fraction to examine the change of the Hadley cell boundaries, since cloudiness is more directly related to precipitating cloud system. Because several studies [*Campbell*, 2004; *Evan et al.*, 2007; *Clement et al.*, 2009] have cautioned about the artifacts in the data, we examined the influence of potential data artifacts on our trend analysis, specifically, the determination of the Hadley cell boundary.

[26] Figure 8 (top) shows the global distribution of trends for the ISCCP cloudiness from 1984 to 2006. Besides an overall decreasing trend in the majority of the tropics and midlatitudes, large negative trends are shown at the outer edge of geostationary satellite footprints, which are mainly

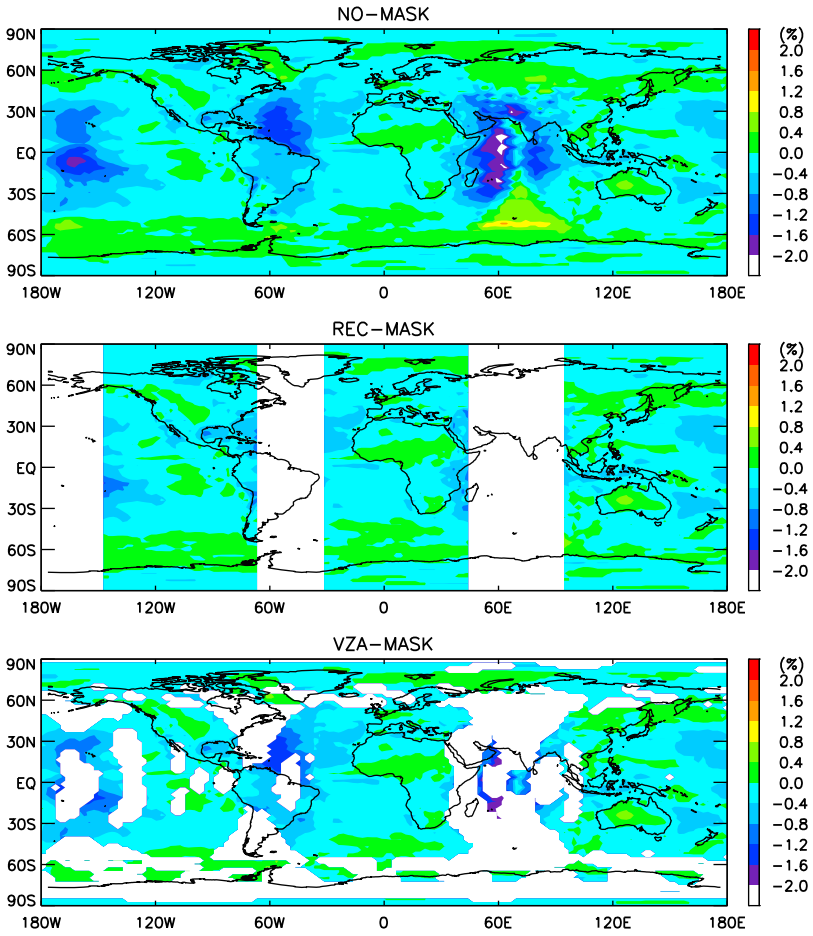

Figure 8. (top) Global distribution of the trends for the ISCCP cloud fraction. (middle) Same as Figure 8 (top) but with three rectangle areas masked. (bottom) Same as Figure 8 (top) but with grids that incur large change of VZA masked.

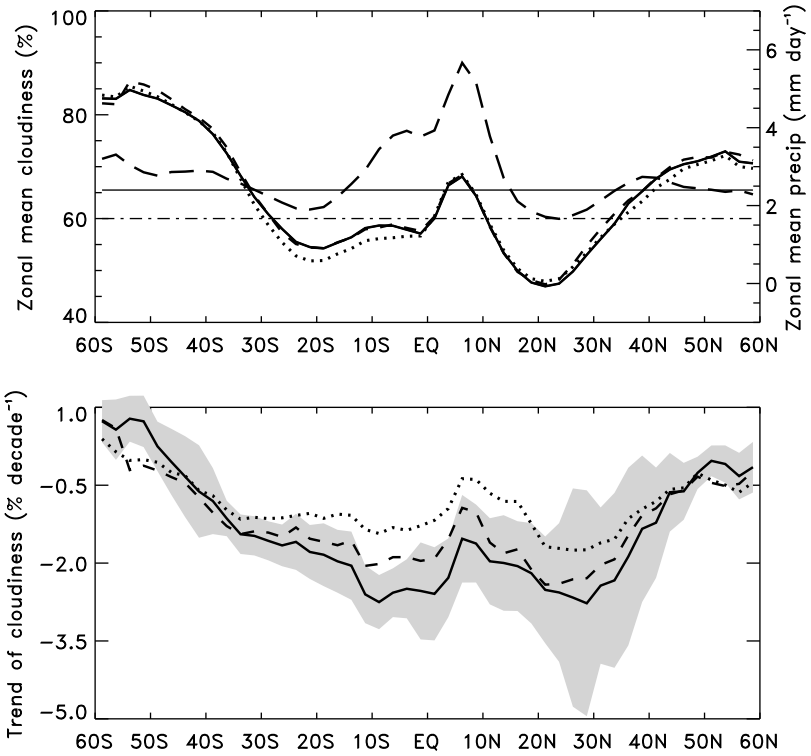

Figure 9. (top) Zonal mean cloud fraction from unmasked (solid line), VZA-masked (short-dashed line), REC-masked (dotted line), as well as zonal mean precipitation (long-dashed line). The 60% cloudiness (dash-dot line) and 2.4 mm d^{-1} threshold (thin solid line) for cloudiness and precipitation are marked with horizontal lines. (bottom) Trends of zonal mean cloudiness from unmasked (solid line), VZA-masked (dashed line), and REC-masked (dotted line) data. The shading indicates error range at 90% level for the solid line.

due to changing satellites, their positions, and the corresponding viewing zenith angles [see also *Evan et al.*, 2007; *Hinkelman et al.*, 2009]. An initial attempt to remove the viewing zenith angle effect by regressing to monthly viewing zenith angle (computed from 3 hourly ISCCP D1 data) at each grid cell only provides limited bias correction because the relationship between cloudiness and viewing zenith angle is complex [*Minnis*, 1989]. Therefore we introduced two types of masks to exclude the regions that are most affected by the changing viewing zenith angles of satellites. The masks are based on a global map of linear trends derived from monthly viewing zenith angle of each grid. One is to remove three rectangle regions (in rectangle (REC) map projection; i.e., three longitudinal bands at 45–90°E, 60–30°W and 150–180°W) that contain large viewing zenith angle and cloudiness changes (REC-mask; see Figure 8, middle); the other is to exclude those grids that have incurred large changes in viewing zenith angle (linear trend of monthly viewing zenith angle (VZA) greater than 0.4 per decade) (VZA-mask; see Figure 8, bottom). Both masks would remove most (if not all) of the biases caused by the changing viewing zenith angles of satellites.

[27] Figure 9 (top) shows zonally averaged cloud fraction using unmasked data (no-mask) as well as the corresponding subsets of data with REC-mask and VZA-mask. Zonal mean precipitation is also plotted in Figure 9. There is almost no change in zonally averaged cloudiness between the unmasked and masked data; this implies for similarly small differences in the mean positions of the Hadley cell and ITCZ boundaries if a nominal threshold of cloudiness is used to determine these boundaries. The peak and low in the zonal mean cloudiness correspond well with the peak and low of zonal mean precipitation. Using 60% cloudiness as threshold, we can roughly define the Hadley cell and ITCZ boundaries as we did for the precipitation.

[28] The Hadley cell boundaries defined by the GPCP precipitation and ISCCP cloudiness are remarkably similar to each other, with the annual mean boundary at ~34°N in the Northern Hemisphere and 31°S and 28°S in the Southern Hemisphere from precipitation and cloudiness data sets, respectively. The mean central positions of the dry band are at 23° and 21° in the Northern Hemisphere, and 22° and 20° in the Southern Hemisphere from the GPCP and ISCCP thresholds, respectively. The ITCZ band, defined by a 60% cloud fraction threshold, is much narrower than that inferred from the precipitation threshold. This is an expected outcome in view of the nonlinear relationship between cloud fraction and precipitation intensity.

[29] The difference in the trends of zonal mean cloudiness between the unmasked and masked data can be seen in Figure 9 (bottom). All three data sets have negative trends between 50°S and 50°N; the unmasked data set has the largest negative trend while REC-masked data has the smallest negative trend owing to the exclusion of large areas

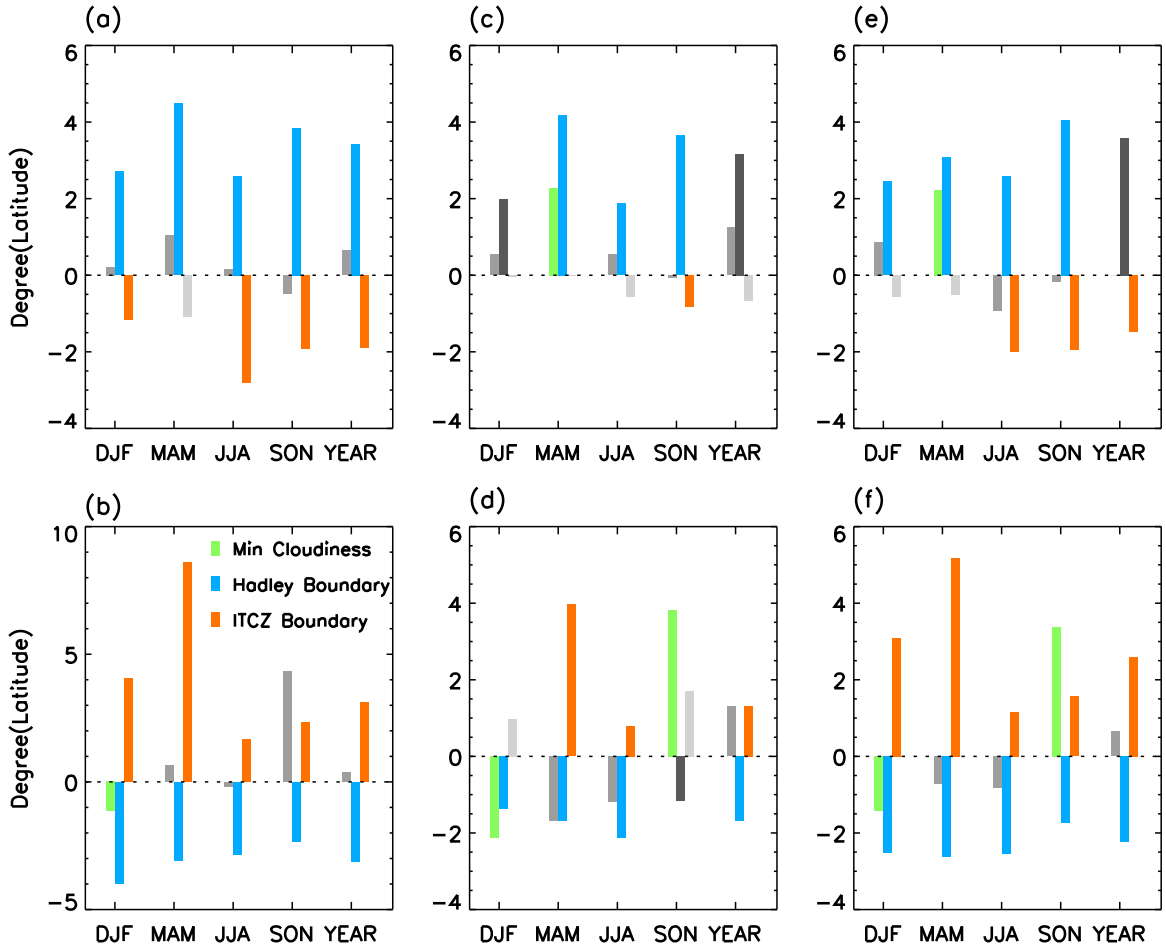

Figure 10. Trends of Hadley cell and ITCZ boundary, as well as the minimum cloudiness derived from using (a and b) unmasked, (c and d) REC-masked, and (e and f) VZA-masked data. The upper and lower panels show trends in the Northern and Southern Hemispheres, respectively. Leftmost, middle, and rightmost bars in each group are for minimum cloudiness, Hadley cell, and ITCZ boundary, respectively. For quantities significant at the 95% level, bars are shaded green, blue, and orange, respectively.

(Figure 8, middle). However, the peaks of negative trends are located around 10°S and 28°N, and neither of them corresponds to the location of annual-mean boundary of ITCZ or Hadley cell defined by nominal cloudiness threshold of 60%. This result implies that the trend analysis will not be influenced much by the artifacts in the ISCCP cloudiness data and one can project that the inferred trends will be quite consistent.

[30] Figure 10 shows the total trends of Hadley cell and ITCZ boundaries defined by the ISCCP cloudiness from unmasked and masked data for the period of 1984–2006. For the unmasked data, the Hadley cell boundary has expanded poleward by ~2–4° degree in both hemispheres with no significant variation with the season. This trend is more robust than that identified with GPCP data, in particular, in the Southern Hemisphere (Figure 5). Also because the ISCCP data period (1984–2006) is slightly shorter than that of GPCP (1979–2007), the changes derived from ISCCP data could multiply by 1.3 (the ratio of the durations of the two periods) if they were to span the GPCP period. The ITCZ boundaries have shifted equatorward in both hemispheres with the largest trends occurring in the hemisphere's fall season, which is somewhat at odds with the trends obtained from GPCP data. This may be result of artifacts in the cloudiness data set since the trends in some seasons are reduced or even reversed in the REC-masked data, in particular, in the Northern Hemisphere (Figures 10c and 10d). It might also be related to changes in low and middle clouds since they do not closely relate to precipitation. Unlike the latitude of minimum precipitation (Figure 5), the latitude of minimum cloudiness does not have a significant trend; it is of the order of a degree in the boreal spring.

[31] The REC-masked (Figures 10c and 10d) and VZA-masked (Figures 10e and 10f) data show slightly smaller trends compared to the unmasked data, but still a significant expansion of the Hadley cell is evident in both hemispheres. The shrinking ITCZ signal is less significant in the REC-masked data than in the VZA-masked data, suggesting that the true trends (if data artifacts were completely removed) in the ITCZ migration and shrinking may not be as robust as the trends in the Hadley cell broadening and poleward migrations.

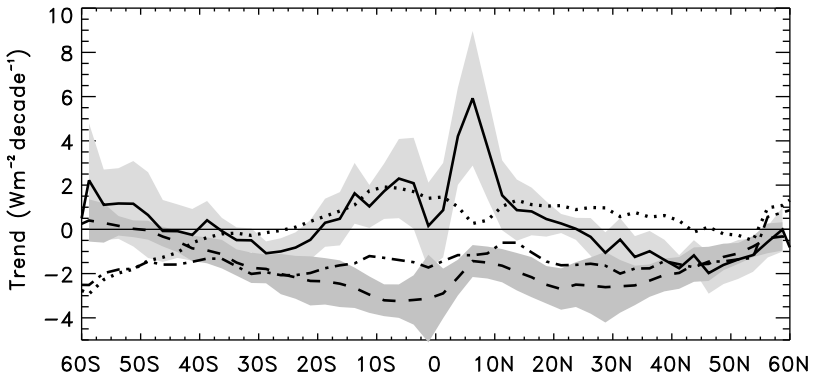

Figure 11. Trends of latent heat (solid line), TOA net radiation (dot-dashed line), OLR (dashed line), and SW (dotted line). Note that the sign of the radiative fluxes is switched to positive for downward fluxes in this plot only. The shadings indicate error range at 90% level for the trends of latent heat and OLR.

4.2. Changing Tropical Hydrological Cycle Inferred From TOA Radiation Components

[32] It is well known that TOA radiation is strongly influenced by atmospheric water vapor, clouds, and precipitation. Since the hydrological cycle and atmospheric radiative forcing are coupled in the tropics [*Betts and Ridgway*, 1989], we attempt to link the observed trends in precipitation with trends in TOA radiation components to obtain additional evidence of the changes in the tropical hydrological cycle. The ISCCP radiation fluxes have been shown to contain minimal artifacts because they are results of many input data sets [*Hinkelman et al.*, 2009], therefore no adjustment is made to the radiation data. Results from excluding the masked areas were similar and hence are not shown.

[33] Figure 11 shows the trend of latent heat release to the atmosphere from precipitation along with the trends of TOA net radiation, outgoing longwave radiation (OLR) and reflected shortwave (SW). The trend of latent heat release to the atmosphere is converted from precipitation trend in millimeters per day per decade by specifying latent heat [$L = 2.5 \times 10^6$ J kg^{-1}]. The trend of latent heat release to the atmosphere is comparable to that of TOA net radiation (note opposite sign in the tropics, and same sign in the subtropics). Even though it is premature to draw quantitative conclusions of the energy balance between latent heating and net TOA radiation, two features are noteworthy. First, the trends in the OLR and SW seem to partially compensate each other as was also found in the ERBE/CERES data for the period of 1985–1989 [*Wong et al.*, 2006]. However, the magnitude of the trend of SW is smaller than that of OLR, resulting in a net loss of energy to space in the tropics, the opposite of the ERBE/CERES data and ISCCP FD data for the 1985–1999 period [*Wong et al.*, 2006]. This is due to the different trends in the 7 years after 1999 (not shown). Second, the increased latent heat in the tropical atmosphere is mainly balanced by increased longwave cooling. Subsequently, we examine the latitudinal distributions of these fluxes and how atmospheric temperature, water vapor, and clouds may have contributed to the trends in total longwave and shortwave heating of the atmosphere.

[34] The trend in all sky fluxes can be decomposed into contributions from changes in clear sky fluxes, cloudy sky fluxes, and cloud fraction according to the following equations:

$$\phi_{all} = \phi_{clr}(1 - f_{cld}) + \phi_{cld} \cdot f_{cld} \tag{1}$$

$$\frac{d\phi_{all}}{dt} = \frac{d\phi_{clr}}{dt}(1 - f_{cld}) + \frac{df_{cld}}{dt}(\phi_{cld} - \phi_{clr}) + \frac{d\phi_{cld}}{dt} f_{cld} \tag{2}$$

where ϕ_{all}, ϕ_{clr} and ϕ_{cld} represent TOA fluxes for all sky, clear sky and cloudy sky conditions, respectively, and f_{cld} is cloud fraction.

[35] The contributions of individual components to the total trends of OLR and TOA reflected SW are shown in Figure 12. For all sky OLR, positive trends are seen over the

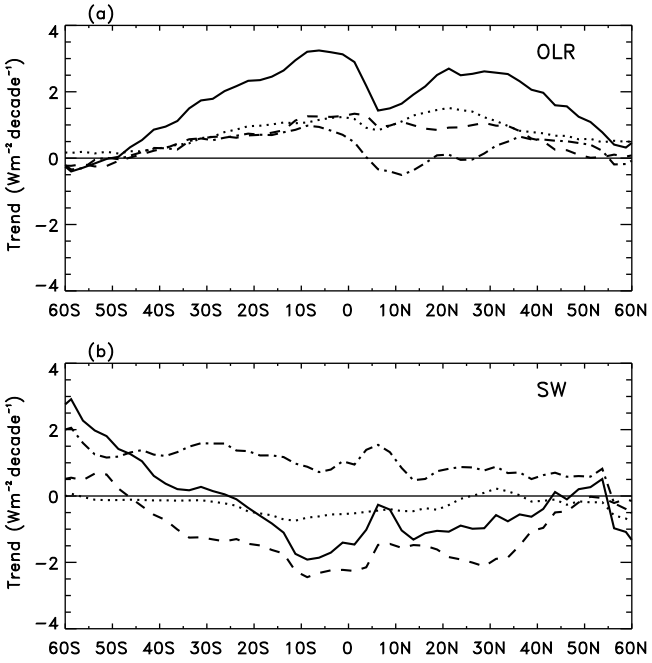

Figure 12. Contributions of changes in TOA clear sky (dotted line), cloudy sky fluxes (dot-dashed line), and cloud fraction (dashed line) to the total trend (solid line) of TOA (a) OLR and (b) reflected SW.

entire tropics and midlatitudes. Roughly one third of the total OLR trend corresponds to the increased clear sky flux (ϕ_{clr}); this comes from near-surface warming that is mitigated by the absorption of longwave by increasing greenhouse gases, primarily CO_2, and water vapor (Figure 12a). Zonal averaged cloudy sky OLR (ϕ_{cld}) shows an increasing (decreasing) trend in the subtropics (ITCZ) that may be the result of a greater proportion of shallow clouds in the subtropical region and deeper clouds in the convective ITCZ regions. This is consistent with increasing strength of the Hadley circulation. Correspondingly, it contributes positively to the total OLR trend in the subtropics but negatively in the deep ITCZ region. The cloud fraction has a negative trend for the entire tropics and midlatitude that peaks in the sinking regions of the Hadley circulation (Figure 9, bottom). It contributes a similar amount to the total OLR trend as the clear sky flux (Figure 12a).

[36] The positive trend in OLR and negative trend of total reflected SW (Figure 12b) in the tropical and subtropical regions is consistent with several previous results [*Wielicki et al.*, 2002; *Chen et al.*, 2002; *Zhang et al.*, 2004; *Wong et al.*, 2006] although the relative strength of the trends, as mentioned earlier, depends upon the data periods and their lengths. The clear sky SW has a decreasing trend for the entire tropics and midlatitudes except near 30°N. This is presumably the result of increased shortwave absorption by the moister atmosphere. The positive trends of cloudy sky SW imply brighter (more reflective) clouds, resulting from increasing strength of the Hadley circulation. In 5–15°N, the negative total SW trend is somewhat weaker than around 15°S owing to relatively smaller reduction of cloud fraction and larger increase of cloud thickness. These changes reveal a warmer and moister atmosphere, reduced cloudiness (more so in the subtropics than in the tropics), greater proportion of shallow clouds in the subtropics and deeper and brighter clouds in the ITCZ regions. These observed changes in cloud and radiation distributions, together with precipitation observations discussed earlier, are intrinsically consistent with a strengthening of the tropical hydrological cycle in recent decades.

5. Summary and Discussion

[37] We have examined decadal trends of the tropical hydrological cycle in the GPCP precipitation and ISCCP cloud and radiation data to determine if such trends can provide an observation-based benchmark for model predictions of the ongoing climate change. Our analysis of GPCP precipitation data revealed that the tropical precipitation trends are related to increasing contrasts between the dry and wet regions; the trends show that the wet regions are getting wetter while the dry regions are getting drier. The tropical Pacific and Atlantic oceans shows increasing (decreasing) precipitation trends in the rising (sinking) regions of the Walker circulation. The Indian Ocean shows significant increasing precipitation in the rising regions of the Walker circulation and statistically insignificant positive change in the sinking region. The precipitation trends associated with the Hadley circulation also show increasing (decreasing) trends in the wetter ITCZ (drier subtropical) regions. These trends indicate a strengthening of the tropical hydrological cycle with intensification of extremes of dry and wet conditions, as discussed in the work of *Chou et al.* [2009].

[38] With a reasonable precipitation threshold to serve as proxy for Hadley cell and ITCZ boundaries, we found that in the last three decades, the zonal mean boundary of Hadley cell has broadened (shifted poleward) in the Northern Hemisphere in all seasons except for MAM, with the largest shift of 6° (or 2° decade^{-1}) in JJA for the 29 year period. The trend in the Southern Hemisphere is comparatively weaker, showing only 1–2° (or 0.3–0.7° decade^{-1}) of poleward shift in JJA and SON. For regional Hadley cells, most regions show poleward shift of the Hadley cell, however, only the Asian continental region shows significant northward shift of the Hadley cell and ITCZ boundaries and expansion of the dry band in the summer season.

[39] The Hadley cell boundaries, if defined by the ISCCP cloud fraction, also show a 2–4° (or 0.9–1.7° decade^{-1}) poleward shift in both hemispheres in the tropics with both biased and bias excluded ISCCP data for the 23 year period. The trends in the ITCZ boundaries may not be as robust as the trends in the Hadley cell broadening because of large discrepancies in the trends derived using masked data and unmasked data. These results provide further credence to earlier findings [*Reichler and Held*, 2005; *Hudson et al.*, 2006; *Hu and Fu*, 2007; *Seidel et al.*, 2008] that suggest a widening of the Hadley cell.

[40] The trends of latent heat to the atmosphere and TOA net radiation show some intrinsic relations of the radiative-convective balance in the atmospheric system [*Allen and Ingram*, 2002]. The trends of ISCCP TOA radiation component fields reflect changes in atmosphere temperature, moisture and cloud that are closely related with precipitation and hydrological cycle. In the subtropical subsidence regions, a large positive OLR trend is also the result of increasing clear sky fluxes, decreasing cloud fraction and increasing proportion of low-level clouds while a small negative trend in the TOA shortwave reflectance is due to increasing moisture absorption, smaller cloud fraction but brighter clouds. In the ITCZ region, deeper and thicker convective clouds reduce the positive OLR and negative SW trends. These results also suggest a decreasing trend of total cloudiness in the tropics (potentially related to tropical warming), an increasing proportion of low-level clouds in the subtropics but deeper and thicker convective clouds in the ITCZ region. All these are consistent with a more vigorous tropical hydrological cycle as inferred from the precipitation field analyses discussed in this study and those in previous studies [*Chen et al.*, 2002; *Wang and Lau*, 2005; *Chou et al.*, 2007; *Zhang et al.*, 2007; *Wentz et al.*, 2007].

[41] We reiterate that strengthening of the tropical hydrological cycle does not necessarily contradict with a predicted weakening tropical overturning circulation [*Vecchi and Soden*, 2007; *Lu et al.*, 2009]. A stronger tropical hydrological cycle could include increasing total precipitation, increasing contrast in precipitation distributions and increasing episodes of intense precipitation and droughts. Such features were identified in other observational [*Trenberth et al.*, 2003; *Gu et al.*, 2007; *Lau and Wu*, 2007; *Allan and Soden*, 2008] and modeling studies [*Meehl et al.*, 2005; *Held and Soden*, 2006; *Chou et al.*, 2007; *Zhang et al.*, 2007; *Meehl et al.*, 2007; *Allan and Soden*, 2008]. We must state that the hydrologic

cycle trends isolated in our study are subject to uncertainties because spatial and temporal inhomogeneities cannot be completely resolved in long-term satellite observations. Therefore, consistent results from multiple independent data and physical insights are most useful in confirming the robustness of the current results.

[42] **Acknowledgments.** Y. P. Zhou was supported by the NASA Precipitation Measurement Mission Program. She thanks W.-K. Lau and A. Y. Hou for their support and valuable discussions. Comments from D. E. Waliser and two anonymous reviewers were very helpful in improving the manuscript. K.-M. Xu and Y. C. Sud are supported by the NASA Modeling, Analysis, and Prediction Program managed by David Considine. Alan Betts acknowledges support from the National Science Foundation under grant AGS-0529797.

References

Adler, R. F., et al. (2003), The Version 2 Global Precipitation Climatology Project (GPCP) monthly precipitation analysis (1979–present), *J. Hydrometeorol.*, *4*, 1147–1167, doi:10.1175/1525-7541(2003)004<1147:TVGPCP>2.0.CO;2.

Allan, R. P., and B. J. Soden (2007), Large discrepancy between observed and simulated precipitation trends in the ascending and descending branches of the tropical circulation, *Geophys. Res. Lett.*, *34*, L18705, doi:10.1029/2007GL031460.

Allan, R. P., and B. J. Soden (2008), Atmospheric warming and the amplification of precipitation extremes, *Science*, *321*, 1481–1484, doi:10.1126/science.1160787.

Allen, M. R., and W. J. Ingram (2002), Constraints on future changes in climate and the hydrologic cycle, *Nature*, *419*, 224–232, doi:10.1038/nature01092.

Betts, A. K. (1998), Climate-convection feedbacks: Some further issues, *Clim. Change*, *39*, 35–38, doi:10.1023/A:1005323805826.

Betts, A. K., and W. Ridgway (1989), Climatic equilibrium of the atmospheric convective boundary layer over a tropical ocean, *J. Atmos. Sci.*, *46*, 2621–2641, doi:10.1175/1520-0469(1989)046<2621:CEOTAC>2.0.CO;2.

Campbell, G. (2004), Viewing angle dependence of cloudiness and the trend in ISCCP cloudiness, paper presented at the 13th Conference on Satellite Meteorology and Oceanography, Am. Meteorol. Soc., Norfolk, Va., 20–23 Sept.

Chen, J., B. E. Carlson, and A. D. Del Genio (2002), Evidence for strengthening of the tropical general circulation in the 1990s, *Science*, *295*, 838–841, doi:10.1126/science.1065835.

Chou, C., and M. Lo (2007), Asymmetric responses of tropical precipitation during ENSO, *J. Climatol.*, *20*, 3411–3433, doi:10.1175/JCLI4197.1.

Chou, C., and J. D. Neelin (2004), Mechanisms of global warming impacts on regional tropical precipitation, *J. Climatol.*, *17*, 2688–2701, doi:10.1175/1520-0442(2004)017<2688:MOGWIO>2.0.CO;2.

Chou, C., J.-Y. Tu, and P.-H. Tan (2007), Asymmetry of tropical precipitation change under global warming, *Geophys. Res. Lett.*, *34*, L17708, doi:10.1029/2007GL030327.

Chou, C., J. D. Neelin, C.-A. Chen, and J.-Y. Tu (2009), Evaluating the "rich-get-richer" mechanism in tropical precipitation change under global warming, *J. Clim.*, *22*, 1982–2005, doi:10.1175/2008JCLI2471.1.

Clement, A. C., R. Burgman, and J. R. Norris (2009), Observational and model evidence for positive low-level cloud feedback, *Science*, *325*, 460–464, doi:10.1126/science.1171255.

Evan, A. T., A. K. Heidinger, and D. J. Vimont (2007), Arguments against a physical long-term trend in global ISCCP cloud amounts, *Geophys. Res. Lett.*, *34*, L04701, doi:10.1029/2006GL028083.

Fu, Q., C. M. Johanson, J. M. Wallace, and T. Reichler (2006), Enhanced mid-latitude tropospheric warming in satellite measurements, *Science*, *312*, 1179, doi:10.1126/science.1125566.

Gu, G. J., R. F. Adler, G. J. Huffman, and S. Curtis (2007), Tropical rainfall variability on interannual-to-interdecadal and longer time scales derived from the GPCP monthly product, *J. Clim.*, *20*, 4033–4046, doi:10.1175/JCLI4227.1.

Held, I. M., and B. J. Soden (2006), Robust responses of the hydrological cycle to global warming, *J. Clim.*, *19*, 5686–5699, doi:10.1175/JCLI3990.1.

Hinkelman, L. M., P. W. Stackhouse Jr., B. A. Wielicki, T. Zhang, and S. R. Wilson (2009), Surface insolation trends from satellite and ground measurements: Comparisons and challenges, *J. Geophys. Res.*, *114*, D00D20, doi:10.1029/2008JD011004.

Hou, Y. A. (1998), Hadley circulation as a modulator of the extratropical climate, *J. Atmos. Sci.*, *55*, 2437–2457, doi:10.1175/1520-0469(1998)055<2437:HCAAMO>2.0.CO;2.

Hu, Y., and Q. Fu (2007), Observed poleward expansion of the Hadley circulation since 1979, *Atmos. Chem. Phys.*, *7*, 5229–5236, doi:10.5194/acp-7-5229-2007.

Hudson, R. D., M. F. Andrade, M. B. Follette, and A. D. Frolov (2006), The total ozone field separated into meteorological regimes—part II: Northern Hemisphere mid-latitude total ozone trends, *Atmos. Chem. Phys.*, *6*, 5183–5191, doi:10.5194/acp-6-5183-2006.

Knutson, T. R., and S. Manabe (1995), Time-mean response over the tropical Pacific to increased CO_2 in a coupled ocean-atmosphere model, *J. Clim.*, *8*, 2181–2199, doi:10.1175/1520-0442(1995)008<2181:TMROTT>2.0.CO;2.

Lau, K. M., and H. T. Wu (2007), Detecting trends in tropical rainfall characteristics, 1979–2003, *Int. J. Climatol.*, *27*, 979–988, doi:10.1002/joc.1454.

Li, H., A. Dai, T. Zhou, and J. Lu (2010), Responses of East Asian summer monsoon to historical SST and atmospheric forcing during 1950–2000, *Clim. Dyn.*, *34*, 501–514, doi:10.1007/s00382-008-0482-7.

Lu, J., G. A. Vecchi, and T. Reichler (2007), Expansion of the Hadley cell under global warming, *Geophys. Res. Lett.*, *34*, L06805, doi:10.1029/2006GL028443.

Lu, J., C. Deser, and T. Reichler (2009), Cause of the widening of the tropical belt since 1958, *Geophys. Res. Lett.*, *36*, L03803, doi:10.1029/2008GL036076.

Lucas, L. E., D. E. Waliser, P. Xie, J. E. Janowiak, and B. Liebmann (2001), Estimating the satellite equatorial crossing time biases in the daily, global outgoing longwave radiation data set, *J. Climatol.*, *14*, 2583–2605, doi:10.1175/1520-0442(2001)014<2583:ETSECT>2.0.CO;2.

Meehl, G. A., J. M. Arblaster, and C. Tebaldi (2005), Understanding future patterns of increased precipitation intensity in climate model simulations, *Geophys. Res. Lett.*, *32*, L18719, doi:10.1029/2005GL023680.

Meehl, G. A., et al. (2007), Global climate projections, in *Climate Change 2007: The Physical Science Basis, Contribution of Working Group I to the Fourth Assessment Report of the Intergovernmental Panel on Climate Change*, edited by S. Solomon et al., pp. 747–845, Cambridge Univ. Press, New York.

Minnis, P. (1989), Viewing zenith angle dependence of cloudiness determined from coincident GOES east and GOES west data, *J. Geophys. Res.*, *94*, 2303–2320, doi:10.1029/JD094iD02p02303.

Mitas, C. M., and A. C. Clement (2005), Has the Hadley cell been strengthening in recent decades?, *Geophys. Res. Lett.*, *32*, L03809, doi:10.1029/2004GL021765.

Mitas, C. M., and A. C. Clement (2006), Recent behavior of the Hadley cell and tropical thermodynamics in climate models and reanalyses, *Geophys. Res. Lett.*, *33*, L01810, doi:10.1029/2005GL024406.

Norris, J. R. (2000), What can cloud observations tell us about climate variability?, *Space Sci. Rev.*, *94*, 375–380, doi:10.1023/A:1026704314326.

Quan, X.-W., et al. (2004), Change of the tropical Hadley cell since 1950, in *The Hadley Circulation: Past, Present, and Future*, edited by H. F. Diaz and R. S. Bradley, pp. 85–120, Cambridge Univ. Press, New York, doi:10.1007/978-1-4020-2944-8_3.

Randall, D. A., M. F. Khairoutdinov, A. Arakawa, and W. W. Grabowski (2003), Breaking the cloud parameterization deadlock, *Bull. Am. Meteorol. Soc.*, *84*, 1547–1564, doi:10.1175/BAMS-84-11-1547.

Reichler, T., and I. Held (2005), Widening trend of the Hadley cell over the past 40 years, paper presented at the Conference on Climate Variability and Change, Am. Meteorol. Soc., Cambridge, Mass., 13–17 June.

Rossow, W. B., and R. A. Schiffer (1999), Advances in understanding clouds from ISCCP, *Bull. Am. Meteorol. Soc.*, *80*, 2261–2287, doi:10.1175/1520-0477(1999)080<2261:AIUCFI>2.0.CO;2.

Santer, B. D., T. M. L. Wigley, J. S. Boyle, D. J. Gaffen, J. J. Hnilo, D. Nychka, D. E. Parker, and K. E. Taylor (2000), Statistical significance of trends and trend differences in layer-average atmospheric temperature time series, *J. Geophys. Res.*, *105*, 7337–7356, doi:10.1029/1999JD901105.

Santer, B. D., et al. (2005), Amplification of surface temperature trends and variability in the tropical atmosphere, *Science*, *309*, 1551–1556, doi:10.1126/science.1114867.

Seidel, D. J., and R. J. Randel (2007), Recent widening of the tropical belt: Evidence from tropopause observations, *J. Geophys. Res.*, *112*, D20113, doi:10.1029/2007JD008861.

Seidel, D. J., Q. Fu, W. J. Randel, and T. J. Reichler (2008), Widening of the tropical belt in a changing climate, *Nat. Geosci.*, *1*, 21–24.

Smith, T. M., X. Yin, and A. Gruber (2006), Variations in annual global precipitation (1979–2004), based on the Global Precipitation Climatology Project 2.5° analysis, *Geophys. Res. Lett.*, *33*, L06705, doi:10.1029/2005GL025393.

Sohn, B. J., and S.-C. Park (2010), Strengthened tropical circulations in past three decades inferred from water vapor transport, *J. Geophys. Res.*, *115*, D15112, doi:10.1029/2009JD013713.

Sud, Y. C., G. K. Walker, Y. P. Zhou, and W. K.-M. Lau (2008), Influence of local and remote sea-surface temperatures on precipitation as inferred from changes in boundary layer moisture convergence and moist thermodynamics over global oceans, *Q. J. R. Meteorol. Soc.*, *134*, 147–163, doi:10.1002/qj.193.

Tanaka, H. L., et al. (2004), Trend and interannual variability of Walker, monsoon and Hadley circulations defined by velocity potential in the upper troposphere, *Tellus, Ser. A*, *56*, 250–269, doi:10.1111/j.1600-0870.2004.00049.x.

Trenberth, K. E., A. Dai, R. M. Rasmussen, and D. B. Parsons (2003), The changing character of precipitation, *Bull. Am. Meteorol. Soc.*, *84*, 1205–1217, doi:10.1175/BAMS-84-9-1205.

Tselioudis, G., E. Tromeur, W. B. Rossow, and C. S. Zerefos (2010), Decadal changes in tropical convection suggest effects on stratospheric water vapor, *Geophys. Res. Lett.*, *37*, L14806, doi:10.1029/2010GL044092.

Uppala, S. M., et al. (2005), The ERA-40 re-analysis, *Q. J. R. Meteorol. Soc.*, *131*, 2961–3012, doi:10.1256/qj.04.176.

Vecchi, G. A., and B. J. Soden (2007), Global warming and the weakening of the tropical circulation, *J. Climatol.*, *20*, 4316–4340, doi:10.1175/JCLI4258.1.

Vecchi, G. A., B. J. Soden, A. T. Wittenberg, I. M. Held, A. Leetmaa, and M. J. Harrison (2006), Weakening of tropical Pacific atmospheric circulation due to anthropogenic forcing, *Nature*, *441*, 73–76, doi:10.1038/nature04744.

Waliser, D. E., and C. Gautier (1993), A satellite-derived climatology of the ITCZ, *J. Clim.*, *6*, 2162–2174, doi:10.1175/1520-0442(1993)006<2162:ASDCOT>2.0.CO;2.

Waliser, D. E., and R. C. J. Somerville (1994), Preferred latitudes of the Intertropical Convergence Zone, *J. Atmos. Sci.*, *51*, 1619–1639, doi:10.1175/1520-0469(1994)051<1619:PLOTIC>2.0.CO;2.

Waliser, D. E., and W. Zhou (1997), Removing satellite equatorial crossing time biases from the OLR and HRC Data Sets, *J. Climatol.*, *10*, 2125–2146, doi:10.1175/1520-0442(1997)010<2125:RSECTB>2.0.CO;2.

Waliser, D. E., Z. Shi, J. R. Lanzante, and A. H. Oort (1999), The Hadley circulation: assessing NCEP/NCAR reanalysis and sparse in-situ estimates, *Clim. Dyn.*, *15*, 719–735, doi:10.1007/s003820050312.

Wang, H., and K. M. Lau (2005), Atmospheric hydrological cycle in the tropics in twentieth century coupled climate simulations, *Int. J. Climatol.*, *26*, 655–678, doi:10.1002/joc.1279.

Webster, P. J., V. O. Magaña, T. N. Palmer, J. Shukla, R. A. Tomas, M. Yanai, and T. Yasunari (1998), Monsoons: Processes, predictability, and the prospects for prediction, *J. Geophys. Res.*, *103*, 14,451–14,510, doi:10.1029/97JC02719

Wentz, F. J., L. Ricciardulli, K. Hilburn, and C. Mears (2007), How much more rain will global warming bring?, *Science*, *317*, 233–235, doi:10.1126/science.1140746.

Wielicki, B. A., et al. (2002), Evidence for large decadal variability in the tropical mean radiative energy budget, *Science*, *295*, 841–844, doi:10.1126/science.1065837.

Wong, T., B. A. Wielicki, R. B. Lee, G. L. Smith, K. A. Bush, and J. K. Willis (2006), Reexamination of the observed decadal variability of the Earth radiation budget using altitude-corrected ERBE/ERBS nonscanner WFOV data, *J. Clim.*, *19*, 4028–4040, doi:10.1175/JCLI3838.1.

Yin, J. H. (2005), A consistent poleward shift of the storm tracks in simulations of 21st century climate, *Geophys. Res. Lett.*, *32*, L18701, doi:10.1029/2005GL023684.

Yu, B., and F. W. Zwiers (2010), Changes in equatorial atmospheric zonal circulations in recent decades, *Geophys. Res. Lett.*, *37*, L05701, doi:10.1029/2009GL042071.

Zhang, M., and H. Song (2006), Evidence of deceleration of atmospheric vertical overturning circulation over the tropical Pacific, *Geophys. Res. Lett.*, *33*, L12701, doi:10.1029/2006GL025942.

Zhang, X., F. W. Zwiers, G. C. Hegerl, F. H. Lambert, N. P. Gillett, S. Solomon, P. A. Stott, and T. Nozawa (2007), Detection of human influence on twentieth-century precipitation trends, *Nature*, *448*, 461–465, doi:10.1038/nature06025.

Zhang, Y., W. B. Rossow, A. A. Lacis, V. Oinas, and M. I. Mishchenko (2004), Calculation of radiative fluxes from the surface to top of atmosphere based on ISCCP and other global data sets: Refinements of the radiative transfer model and the input data, *J. Geophys. Res.*, *109*, D19105, doi:10.1029/2003JD004457.

Zhao, H., and G. W. K. Moore (2008), Trends in the boreal summer regional Hadley and Walker circulations as expressed in precipitation records from Asia and Africa during the latter half of the 20th century, *Int. J. Climatol.*, *28*, 563–578, doi:10.1002/joc.1580.

Zhao, P., S. Yang, and R. Yu (2010), Long-term changes in rainfall over eastern China and large-scale atmospheric circulation associated with recent global warming, *J. Climatol.*, *23*, 1544–1562, doi:10.1175/2009JCLI2660.1.

A. K. Betts, Atmospheric Research, 58 Hendee Ln., Pittsford, VT 05763, USA.

Y. C. Sud and Y. P. Zhou, Laboratory for Atmospheres, NASA Goddard Space Flight Center, Code 613.2, Greenbelt, MD 20771, USA. (yaping.zhou-1@nasa.gov)

K.-M. Xu, Climate Science Branch, Science Directorate, NASA Langley Research Center, Hampton, VA 23681-0001, USA.